Inorganic Chemistry

Article

pubs.acs.org/IC

Small is Beautiful: The Unusual Transformation of Nanocrystalline Layered α-Zirconium Phosphate into a New 3D Structure

Monica Pica,*[,†] Riccardo Vivani,[†] Anna Donnadio,[†] Elisabetta Troni,[‡] Sacha Fop,[§] and Mario Casciola[‡]

[†]Department of Pharmaceutical Sciences and [‡]Department of Chemistry, Biology, and Biotechnologies, University of Perugia, 06123 Perugia, Italy

[§]The Chemistry Department, University of Aberdeen, Meston Building, , AB24 3UE Aberdeen, Scotland, U.K.

Supporting Information

ABSTRACT: Nanosized α-zirconium phosphate, α-ZrP, undergoes a phase transition at 120 °C, which is not observed with microcrystalline α-ZrP in the same conditions, and which leads to a new 3D phase. The new compound, with formula $Zr(HPO_4)_2$ (τ′-ZrP), consists of cubelike nanoparticles and has a tetragonal unit cell (space group $P4_32_12$, a = 7.955 Å, c = 10.744 Å). The structure of τ′-ZrP is in close relationship with that of the already known τ-ZrP. Both structures are made of packed chains of eight-membered rings, composed of Zr atoms connected to bridging HPO_4 groups. The main difference between the two structures concerns the different orientation of the uncoordinated P−OH groups, pointing into the channels. The in situ XRPD analysis on nanosized α-ZrP, performed at 120 °C as a function of time, provided information about the kinetics of the formation of τ′-ZrP, showing that the α-ZrP phase is directly transformed into τ′-ZrP. Moreover, τ′-ZrP is converted into α-ZrP at room temperature in the presence of water vapor. It was proved that the free phosphoric acid, which is originally present in small amounts in nanosized α-ZrP and τ′-ZrP, is necessary for the interconversion between the two phases. As a matter of fact, the removal of phosphoric acid, by washing α-ZrP and τ′-ZrP with anhydrous ethanol, inhibits the above conversion.

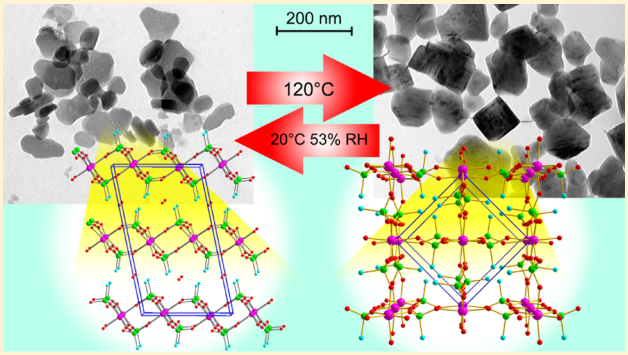

1. INTRODUCTION

Layered zirconium phosphates (ZrP) are a class of well-known and versatile materials, due to their ion-exchange and intercalation properties[1] associated with high thermal stability and excellent chemical inertia in strong acidic media. The α- and γ-types of ZrP, with formulas of $α\text{-}Zr(HPO_4)_2·H_2O$ and $γ\text{-}ZrPO_4(H_2PO_4)·2H_2O$, respectively, are the most representative layered compounds that have been employed as ion exchangers, polymer fillers, solid-state proton conductors, catalysts, and drug delivery systems.[2] It is known that the size and morphology of the zirconium phosphate crystals can be tuned according to two main strategies: (a) by changing the synthesis parameters such as reagent concentrations, temperature, time, solvent, etc,[2h,3] and (b) by a suitable postsynthesis treatment.[2g,j,n] Recently, it was found that the reaction between phosphoric acid and a zirconyl organic salt in aliphatic alcohol media allows to quickly obtain gels of alcohol-intercalated α-ZrP nanocrystals.[3a] Nanocrystalline α-ZrP so obtained was found to show different physical−chemical properties as compared to conventional microcrystalline α-ZrP. For example, nanocrystalline α-ZrP gel is much more reactive toward postsynthesis treatments than the microcrystalline analogue, allowing the preparation of single-phase mixed zirconium phosphate phosphonate compounds by simple topotactic anion exchange reactions, at room temperature;[4] furthermore, it easily disperses within polymer matrices, thus forming polymeric nanocomposites with highly improved mechanical properties.[4a,5] Therefore, the gel procedure represents an innovative, versatile, and mild approach for the synthesis of ZrP nanoparticles. We recently found that nanosized α-ZrP also has a different thermal behavior as compared with microcrystalline α-ZrP. This latter material undergoes a first phase transition at T > 100 °C, due to dehydration, and a second reversible phase transition at T > 220 °C leading to an hexagonal phase. The typical α-type structure of the layers is retained at least up to 600 °C, where condensation to zirconium pyrophosphate starts to occur.[1] On the contrary, nanosized α-ZrP undergoes a phase transition with formation of a new ZrP phase with a three-dimensional (3D) structure at only 120 °C. The present paper aims to thoroughly investigate the thermal behavior of nanosized α-ZrP to elucidate the conditions leading to this new phase, as well as its structural features and stability.

2. EXPERIMENTAL SECTION

2.1. Chemicals. Zirconyl propionate $(ZrO_{1.26}(C_2H_5COO)_{1.49}$, FW = 220 Da) was supplied by Magnesium Elektron Ltd., England.

Received: July 14, 2015
Published: August 31, 2015

DOI: 10.1021/acs.inorgchem.5b01573
Inorg. Chem. 2015, 54, 9146−9153

Concentrated orthophosphoric acid (85%, 14.8 M) was supplied by Fluka. Propanol was purchased from Carlo Erba. All other reagents were supplied by Aldrich.

2.2. Preparation of the ZrP Gels in Alcohol. Gels of nanosized ZrP in aliphatic alcohols were prepared according to the "gel method".[3a] Specifically, 3.3 mmol of zirconyl propionate were dissolved in 10 mL of anhydrous alcohol (ethanol, propanol, butanol). Concentrated phosphoric acid (0.45, 0.90, and 1.35 mL, respectively) was added, at room temperature under stirring, to the above solution so that the H_3PO_4/Zr molar ratio (R) was 2, 4, and 6, respectively, and [H_3PO_4] was in the range of 0.7−2.0 M.

Clear solutions were obtained just after mixing, which turned into gels in a few minutes. Transparent gels were obtained for $R > 2$. The gels thus obtained were washed three times with the same alcohol used for the synthesis.

Powdered samples were obtained by drying the gels in an oven at 60 or 120 °C until complete solvent elimination (15 h). Hereafter the gel samples will be labeled as *alcohol_R_gel*, and dry powders obtained from the gels will be labeled as *alcohol_R_T*, where *alcohol* is the solvent of the gel, R is the H_3PO_4/Zr molar ratio, and T is the drying temperature of the gels.

2.3. Techniques. X-ray powder diffraction (XRPD) patterns of gels and powders were collected with a Panalytical X'Pert PRO MPD diffractometer operating at 40 kV and 40 mA, with a step size of 0.03° and step scan of 25 s, using Cu Kα radiation and an X'Celerator detector.

Transmission electron microscopy (TEM) analysis was performed by a Philips 208 transmission electron microscope, operating at an accelerating voltage of 100 kV. Powders were rapidly diluted in ethanol and sonicated for a few minutes, then supported on copper grids (200 mesh) precoated with Formvar carbon films, and quickly dried.

The (P/Zr) molar ratio of the powder samples was determined by using a Varian Liberty Series inductively coupled plasma-optical emission spectrometer (ICP-OES) with axial injection. A weighted amount of the samples was dissolved in 3 M HF (~0.2 mL) and then diluted with water.

2.4. Structure Determination and Refinement for τ'-ZrP. Unit cell parameters were determined using both TREOR90[6] and DICVOL91[7] programs. For this, a preliminary peak-profile fitting, using pseudo-Voigt functions for the determination of the position of Kα_1 maxima, was performed.

The structure was solved in the direct space under the $P4_32_12$ space group (No. 96) with a "Reverse Monte Carlo" method implemented in the FOX program.[8] Trial structures were generated using the "Parallel Tempering" algorithm.[9] The structure was described using one ZrO_6 octahedron and one PO_4 tetrahedron as building blocks. Hydrogen atoms were omitted. Starting values for bond lengths and angles were taken from similar systems found in the literature and constrained within standard deviations of 0.15 Å and 10°, respectively.

The model obtained with the above procedure was then refined using the Rietveld method performed with the GSAS program.[10] At the end of the refinement, the shifts in all parameters were less than their standard deviations. Crystal data and details of the refinement are reported in Table 1.

Table 1. Crystal Data and Refinement Details for τ'-$Zr(HPO_4)_2$

empirical formula	$ZrP_2O_8H_2$
formula weight	283.2
crystal system	tetragonal
space group	$P4_32_12$
a/Å	7.9546(1)
c/Å	10.7392(2)
V/Å^3	679.54(1)
Z	8
T/K	298
ρ_{calc}/g cm^{-3}	2.77
2θ range for data collection/deg	13−120
step scan increment, 2θ/deg	0.017
step scan time/s	90
reflections collected, unique	333
data, parameters	6294, 48
geometrical constraints	23
R_p[a]	0.039
R_{wp}[b]	0.054
R_F2[c]	0.083
χ[d]	2.59

[a] $R_p = \sum|I_o - I_c|/\sum I_o$. [b] $R_{wp} = [\sum w(I_o - I_c)^2/\sum wI_o^2]^{1/2}$. [c] $R_F2 = \sum|F_o^2 - F_c^2|/\sum|F_o^2|$. [d] $\chi = [\sum w(I_o - I_c)^2/(N_o - N_{var})]^{1/2}$.

3. RESULTS AND DISCUSSION

The structure of monohydrated α-ZrP is monoclinic: each layer is made of a plane of Zr atoms arranged in a pseudohexagonal symmetry, and bridged to monohydrogen phosphate groups, pointing above and below this plane; the water molecules located in the interlayer region form hydrogen bonds with the phosphate groups.[1]

α-ZrP nanoparticles obtained with the "gel method" (*alcohol_R_gel* samples, see Experimental Section) have an almost regular shape and planar size of some tens of nanometers. When the gels are dried at 60 °C, the ZrP particles tend to grow, thus obtaining the *alcohol_R_60* samples, with particles having planar size of some hundreds of nanometers. The following general formula was assigned to both *alcohol_R_gel* and *alcohol_R_60* samples: $Zr(OH)_w(HPO_4)_x(H_2PO_4)_y{\cdot}zH_3PO_4$, showing that, besides bidentate H_2PO_4, tridentate HPO_4, and hydroxyl groups bonded to Zr(IV), free phosphoric acid is also present; as an example, for *propanol_6_60* it was found that $w = 0.16$, $x = 1.8$, $y = 0.24$, and $z = 0.26$. It was also observed that the *alcohol_R_60* samples contained a higher amount of HPO_4 and H_3PO_4 groups as compared to the corresponding *alcohol_R_gel* samples: it was inferred that, during the drying process, the H_2PO_4 groups reacted giving HPO_4 and H_3PO_4.[3a] The chemical−physical features of both gels and nanocrystalline powders proved to be affected by several parameters, among which were the R value and the kind of aliphatic alcohol used as solvent. Specifically, the highest degree of crystallinity was achieved for $R = 6$ and butanol as solvent.

More recently, we discovered that also the temperature set for the solvent evaporation played a role on the formation of the corresponding compounds. As an example, the XRPD patterns of *propanol_6_60* and *propanol_6_120* are reported in Figure 1a,c; it can be observed that they are completely different.

Specifically, the pattern of *propanol_6_60* shows the typical peaks of the layered α-ZrP·H_2O phase; differently, the pattern of *propanol_6_120* is very similar to that of a compound that was described for the first time by Clearfield et al.[11] in 1973 and Segawa et al.[12] in 1985 and whose crystal structure was determined by Krogh-Andersen et al.[13] in 1998. That phase, indicated as τ-$Zr(HPO_4)_2$ (hereafter τ-ZrP), had the same composition of anhydrous α-ZrP, but exhibited a 3D framework structure. Similar patterns were obtained for *ethanol_6_120* and *butanol_6_120*.

However, a detailed comparison of the two patterns (Figure 1c,d) allowed us to find some relevant differences, even though involving peaks of low intensity: in particular, the absence in the new phase of the peaks at 19.62, 30.58, and 33.84° 2θ and the presence of a new peak at 17.82° 2θ, not observed in τ-ZrP.

DOI: 10.1021/acs.inorgchem.5b01573
Inorg. Chem. 2015, 54, 9146−9153

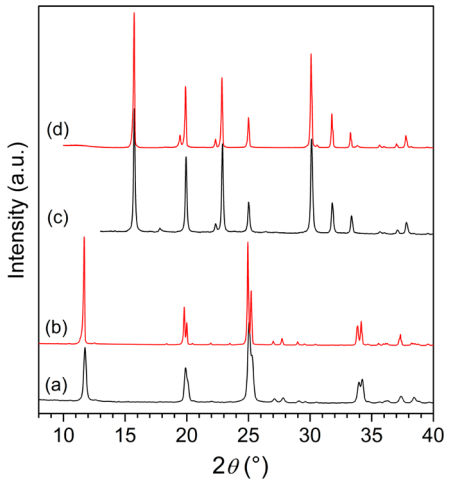

Figure 1. XRPD patterns of *propanol_6_60* (a), microcrystalline α-$Zr(HPO_4)_2{\cdot}H_2O$ (b), *propanol_6_120* (c), and microcrystalline τ-$Zr(HPO_4)_2$ (d). (b, d) Reported for comparison.

Note that this last peak is not included in the set of possible diffraction peaks of τ-ZrP structure.

To verify if these discrepancies could be due more to impurities and effects related to sample preparation for XRPD analysis than to a different crystal structure, the sample was thoroughly investigated from a crystallographic point of view. First of all, the absence of the above-mentioned peaks was confirmed by using different procedures for sample loading, to exclude an effect of preferred orientation of microcrystals. Furthermore, an autoindexing procedure was performed to verify if all peaks could be described by one unit cell, or if the new peak should be attributed to an impurity.

The indexing procedure, performed as described in the Experimental Section, gave a tetragonal unit cell with parameters a = 7.955 Å and c = 10.744 Å as a very robust solution, because all peaks were indexed with a high figure of merit: M(20) = 49.[14] The refined unit cell parameters are reported in Table 1. The found unit cell clearly is in close relationship with that of τ-ZrP (tetragonal, space group: $I4_1cd$, a = 11.259(1) Å, c = 10.764(1) Å). Given a', c', and V', the lattice parameters for τ-ZrP, those of the new phase, a, c, and V, can be found by the following equations: $a = a' \times \sqrt{2}/2$; $c = c'$; $V = 1/2V'$. These results, together with the fact that the XRPD patterns of the two phases globally are very similar, suggested to us the possibility that the new phase could be originated by a symmetry decrease in the structure of τ-ZrP. The analysis of the indexed pattern clearly revealed the presence of the following limiting reflection conditions: 00l, l = 4n, and h00, h = 2n, which suggested $P4_32_12$ as the probable space group. In addition, a systematic comparison of the number of peaks found and the number of possible peaks, in all tetragonal space groups using the Chekcell program,[15] estimated $P4_32_12$ as the best choice. Ab initio structure determination and Rietveld refinement, under this space group, essentially confirmed this hypothesis. Since the structure of this new phase is very similar to that of τ-ZrP, it will be indicated in the following as τ′-ZrP. Figure 2 shows the final Rietveld and difference plot. Figure 3 shows a comparison of the structures of τ- and τ′-ZrP, in which the relationships between their unit cells are evident.

Both of these structures have the same connectivity of ZrO_6 octahedra coordinated with six HPO_4 tetrahedra; each tetrahedron is tridentate, connecting three different Zr atoms,

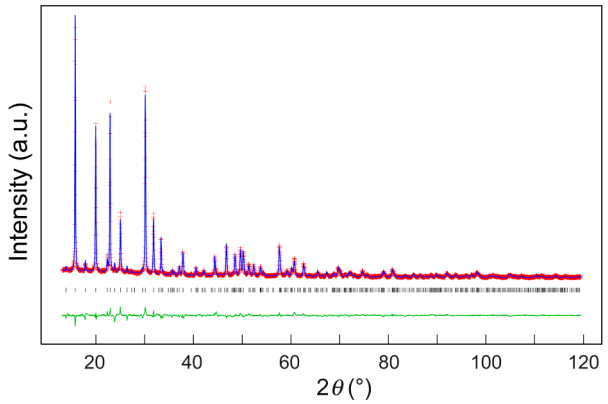

Figure 2. Final Rietveld and difference plot for τ′-ZrP.

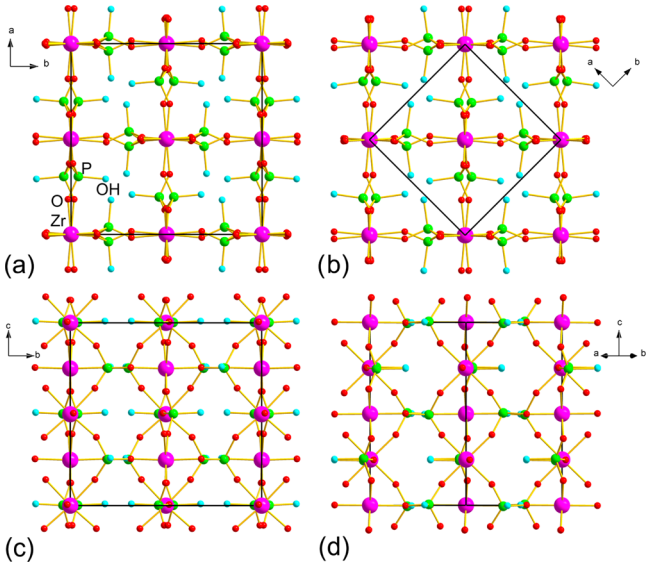

Figure 3. Structure of (a) τ-ZrP and (b) τ′-ZrP viewed along the c axis and along the ab plane ((c) and (d), respectively).

for the formation of a 3D framework. However, apart from some small differences on bond lengths and angles (reported in Table 2), main changes can be found in the orientation of HPO_4 groups. To better explain this aspect, we may consider the structure of τ′-ZrP as composed of primary chains, running along the c axis made of the sequence of Zr octahedra connected, in their equatorial plane, to bridging HPO_4 tetrahedra, with the formation of eight-membered rings (Figure 4a,b).

The whole structure can be seen as the packing of these parallel chains oriented with their main planes perpendicular to each other, as depicted in Figure 4c,d. The third P−O group of each HPO_4 tetrahedron covalently joins the adjacent chain.

The residual uncoordinated P−OH groups are placed roughly perpendicular to the chain plane and point alternately above and below this plane. The structure of τ-ZrP can be described in a similar way. But, in τ-ZrP each eight-membered ring, of which the chain is composed, contains two facing P−OH groups pointing above and below the chain plane, as shown in Figure 5a, while in τ′-ZrP each eight-membered ring contains two P−OH groups pointing to the same side of the plane chain, while in the successive ring they point to the opposite side (Figure 5b).

DOI: 10.1021/acs.inorgchem.5b01573
Inorg. Chem. 2015, 54, 9146−9153

Table 2. Selected Bond Lengths and Angles for τ'-$Zr(HPO_4)_2$

bond	length (Å)	angle	amplitude (deg)
Zr–O1	2.037(4)	O1–Zr–O1	90.1(4)
Zr–O2	2.091(5)	O1–Zr–O2	90.6(2)
Zr–O3	2.086(4)	O1–Zr–O2	179.24(4)
P–O1	1.479(5)	O1–Zr–O3	95.3(3)
P–O2	1.515(6)	O1–Zr–O3	92.2(3)
P–O3	1.488(5)	O2–Zr–O2	88.7(4)
P–O4	1.727(5)	O2–Zr–O3	88.0(3)
O4···O4	2.927(3)	O2–Zr–O3	84.3(3)
		O3–Zr–O3	169.3(4)
		O1–P–O2	111.3(4)
		O1–P–O3	113.1(5)
		O1–P–O4	112.6(6)
		O2–P–O3	104.2(5)
		O2–P–O4	110.1(6)
		O3–P–O4	104.9(4)
		Zr–O1–P	157.1(6)
		Zr–O2–P	153.4(5)
		Zr–O3–P	151.3(4)

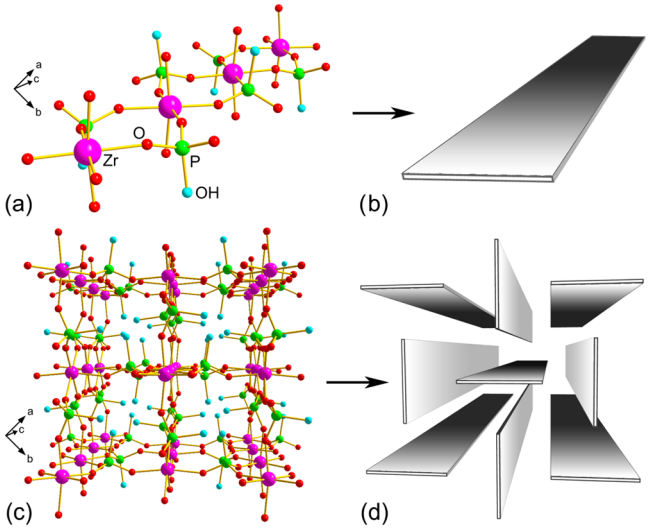

Figure 4. Scheme of the structure of τ'-ZrP as composed of primary chains (a, b) and their reciprocal orientation in the structure packing (c, d).

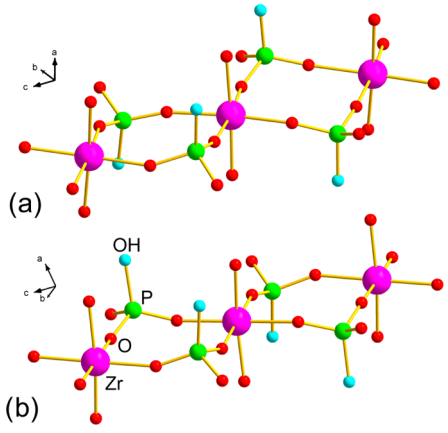

Figure 5. Scheme of different orientation of P–OH groups in τ-ZrP (a) and τ'-ZrP (b).

Also in τ'-ZrP, P–OH groups are pointing into channels extending along the c axis and form a continuous spiral path of H-bonds along the 4_3 axis. (O4···O4 bond distance = 2.927(3) Å).

Figure 6a shows a representative TEM image of the *propanol_6_60* sample, consisting of flat and very thin particles

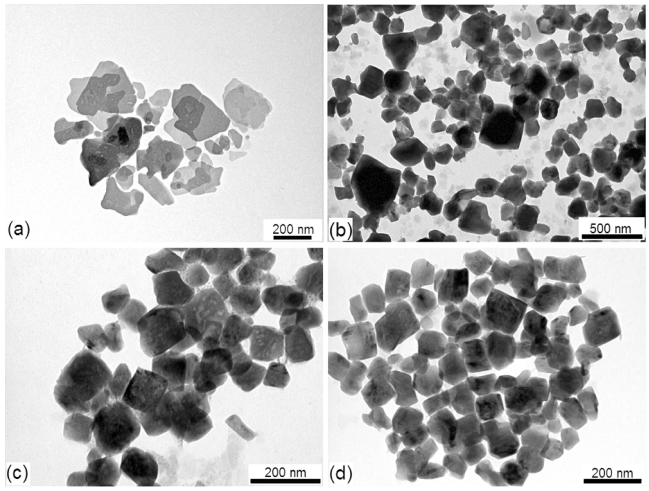

Figure 6. Representative TEM images of *propanol_6_60* (a), *ethanol_6_120* (b), *propanol_6_120* (c), and *butanol_6_120* (d) samples.

with an irregular shape and size from tens to hundreds of nanometers. The *alcohol_6_120* samples exhibit a completely different morphology, consisting of pseudocubic nanoparticles with a more homogeneous shape and size distribution, ranging from 100 to 500 nm (Figure 6b–d).

Owing to the strong structural similarity of τ-ZrP and τ'-ZrP, one should assume that they also have similar chemical properties. In this regard, it is known that τ-ZrP can be prepared in a very narrow window of conditions that are very close to those for cubic zirconium pyrophosphate, ZrP_2O_7: high temperatures (~190 °C), highly concentrated H_3PO_4, and reaction time of several days (4–6).

On the contrary, τ'-ZrP is obtained simply by solvent evaporation from the *propanol_6_gel* sample at 120 °C: this behavior is really unexpected and surprising. To our knowledge, no examples are reported in the literature showing the conversion of an α-type ZrP structure, which essentially constitutes the *propanol_6_gel* sample, into a τ-type ZrP phase, in pretty mild conditions. By the way, structural relationships between α-ZrP and τ'-ZrP phases are not obvious, and a simple interconversion mechanism can be hardly predicted from crystal structure comparison.

In summary, although we are still not able to deeply explain why τ'-ZrP can be formed so easily, it is possible to ascribe this behavior to the special reactivity of nanocrystalline α-ZrP gel. In this regard, it has been already observed that the particle size and crystallinity can affect some reactivity features, such as ion exchange behavior, of zirconium phosphates.[16]

Further experiments, to deeply investigate the formation of the τ'-ZrP nanocrystals, were performed by using the *propanol_R_gel* samples as starting materials.

Figure 7 shows the XRPD patterns of the *propanol_R_120* samples, obtained by heating the corresponding *propanol_R_gel* samples at 120 °C for 15 h. The formation of the τ'-ZrP phase was observed starting from *propanol_6_gel* (*propanol_6_120*

DOI: 10.1021/acs.inorgchem.5b01573
Inorg. Chem. 2015, 54, 9146–9153

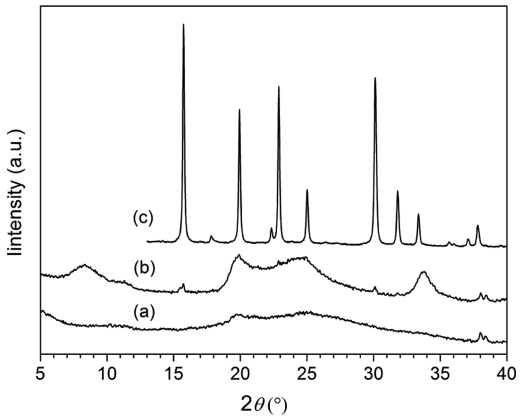

Figure 7. XRPD patterns of *propanol_2_120* (a), *propanol_4_120* (b), and *propanol_6_120* (c).

sample, pattern (c)). On the contrary, *propanol_2_120* is basically amorphous, while the pattern of *propanol_4_120* shows four main broad peaks, which can be reasonably attributed to layered α-ZrP with residual solvent molecules intercalated in the interlayer region; a small amount of τ'-ZrP is also formed, as suggested by the presence of the two weak peaks, at 15.7 and 31.1° 2θ. Therefore, it can be inferred that the formation of the pure τ'-ZrP crystalline phase, by heating the *propanol_R_gel* compounds at 120 °C, occurred only for R values >4.

The effect of the heating time on the formation of τ'-ZrP from *propanol_6_gel* was also investigated. With this aim, XRPD patterns were collected at a given heating time, and the results are shown in Figure 8.

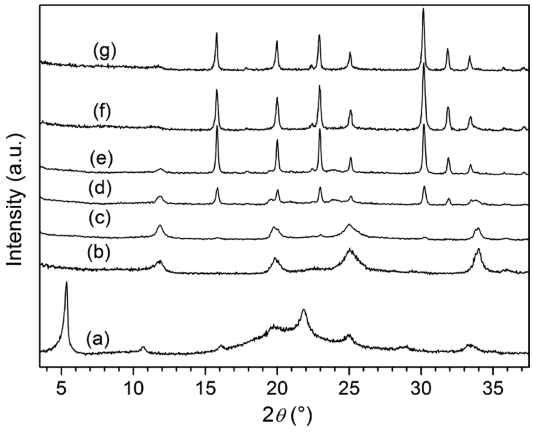

Figure 8. XRPD patterns, taken at 25 °C, of *propanol_6_gel*, after the following heating times (min) at 120 °C: 0 (a), 30 (b), 60 (c), 120 (d), 180 (e), 270 (f), 960 (g).

The XRPD pattern of *propanol_6_gel* collected at room temperature corresponds to that of the α-ZrP·2PrOH intercalation compound[3a] (Figure 8a). The pattern in Figure 8b, collected after 30 min of heating, still shows the presence of the reflection at 33.8°2θ, which is characteristic of α-type ZrP phases, while the first peak shifts from d = 16.1 Å to $d \approx$ 7.5 Å, indicating the deintercalation of propanol upon heating. By heating the *propanol_6_gel* for 60 min, the typical reflections of τ'-ZrP appeared, and after 270 min the α-ZrP phase is completely disappeared.

The above results suggest the following reaction scheme:

$$\alpha\text{-ZrP·2PrOH} \xrightarrow{-2\text{PrOH}} \alpha\text{-ZrP} \xrightarrow{120\,^\circ\text{C}} \tau'\text{-ZrP}$$

A structural evolution study as a function of the time was also performed with an in situ XRPD analysis using a high-temperature chamber maintained at 120 °C. In this case the starting material was a powder *propanol_6_60* sample, because gel samples, undergoing strong dimensional changes during heating, could not be used. The XRPD patterns, collected at specific heating times, are shown in Figure 9.

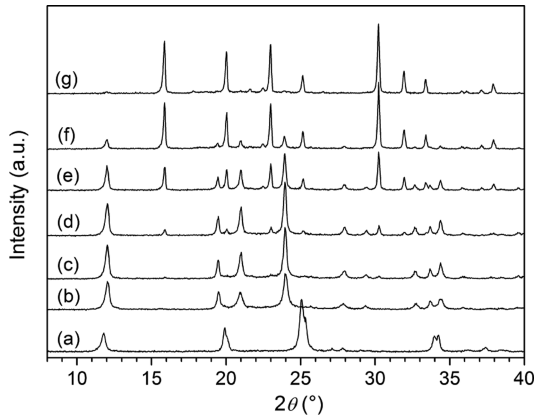

Figure 9. XRPD patterns of *propanol_6_60* at 25 °C (a) and 120 °C after the following heating times (min): 30 (b), 180 (c), 300 (d), 630 (e), 1290 (f), 2250 (g).

The data collected by in situ XRPD analysis indicate that the formation of the τ'-ZrP phase also occurs by thermal treatment of *propanol_6_60*. Note that the formation of the τ'-ZrP phase from *propanol_6_60* is slower than from *propanol_6_gel*. Specifically, after 30 min of heating at 120 °C, the α-ZrP·H_2O phase transforms into anhydrous α-ZrP, having an interlayer distance of 7.41 Å (pattern (b)). After 180 min of heating at 120 °C, the typical peaks of the τ'-ZrP phase appeared (pattern (c)). It was also observed that, while the peak intensity of the anhydrous α-ZrP phase decreased, that of the τ'-ZrP phase increased; thus, after 2250 min of heating, anhydrous α-ZrP can be considered completely disappeared, and only τ'-ZrP is observed.

The above results suggested the following reaction scheme:

$$\alpha\text{-ZrP·H}_2\text{O} \xrightarrow{120\,^\circ\text{C}} \text{anhydrous } \alpha\text{-ZrP} \xrightarrow{120\,^\circ\text{C}} \tau'\text{-ZrP}$$

A kinetic study of the α-ZrP → τ'-ZrP transformation was performed by considering the integrated intensity of the peak at 12.0°2θ for anhydrous α-ZrP (I_t) and that of the peak at 15.9°2θ for τ'-ZrP (I'_t); these integrated intensities were used to calculate the following mass fractions, $\alpha_{\alpha\text{-ZrP}}$ and $\alpha_{\tau'\text{-ZrP}}$:

$$\alpha_{\alpha\text{-ZrP}} = \frac{I_t}{I_0}$$

$$\alpha_{\tau'\text{-ZrP}} = \frac{I'_t}{I'_0}$$

where I_0 and I'_0 are the maximum integrated intensities of anhydrous α-ZrP and τ'-ZrP, calculated at t = 30 min and t = 2250 min of heating time, respectively. By plotting $\alpha(t)$ versus the time, an s-shaped profile was observed, as shown in Figure 10. The kinetics of formation of τ'-ZrP is similar to the shape of

DOI: 10.1021/acs.inorgchem.5b01573
Inorg. Chem. 2015, 54, 9146−9153

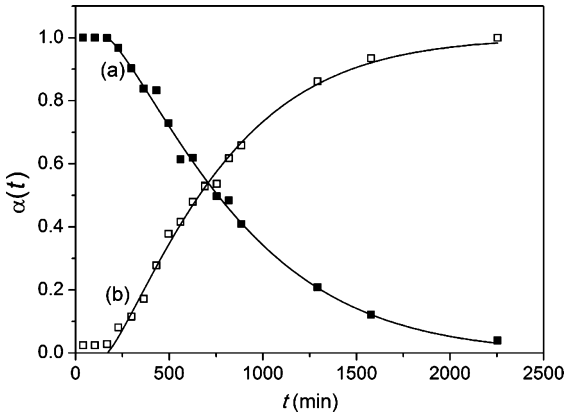

Figure 10. Phase fractions of anhydrous α-ZrP (a) and τ'-ZrP (b) during heating at 120 °C, and fits with the JMAK eqs 1 and 2.

the Johnson–Mehl–Avrami–Kolmogorov (JMAK) kinetics,[17] which is used to describe crystallization processes, phase transistions, and solid-state reactions. The kinetic data of Figure 10 reveal that the appearance of τ'-ZrP and also the disappearance of anhydrous α-ZrP did not start at the reaction time $t = 0$, but there is an incubation time, t_0, after which the mass fraction of the two phases starts to change. In light of this, the experimental kinetic data for τ'-ZrP can be fitted by the following JMAK equation:

$$\alpha_{\tau'\text{-ZrP}} = 1 - \exp(-(k(t - t_0))^n) \quad (1)$$

where k and n are fitting parameters, while t_0 is not a fitting parameter but was estimated from Figure 10 (t_0 = 168 min). If the anhydrous α-ZrP phase changes directly into the τ'-ZrP phase, then the mass fraction $\alpha_{\alpha\text{-ZrP}}$ can be expressed as follows:

$$\alpha_{\alpha\text{-ZrP}} = 1 - \alpha_{t\prime\text{-ZrP}} = \exp(-(k(t - t_0))^n) \quad (2)$$

The analysis of the kinetic data of Figure 10 was performed by using the so-called Sharp–Hancock method, that is, by plotting $\ln(-\ln(1 - \alpha_{\tau'\text{-ZrP}}))$ (or $\ln(-\ln(\alpha_{\alpha\text{-ZrP}}))$) versus $\ln(t - t_0)$; the obtained linear plots are reported in Figure 11.

The Sharp–Hancock plots provided the following information:

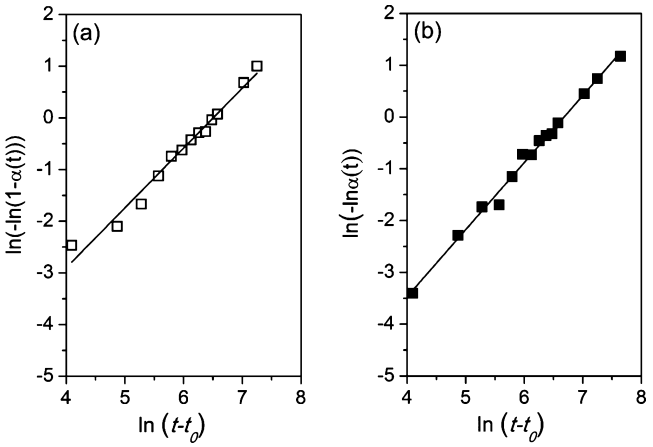

Figure 11. Sharp–Hancock plots for (a) $\alpha_{\tau'\text{-ZrP}}$ (eq 1) and (b) $\alpha_{\alpha\text{-ZrP}}$ (eq 2).

- The experimetal data can be interpolated by single linear functions, thus indicating that there is no change in the reaction mechanism for the two systems;
- The fitting parameters for α-ZrP and τ'-ZrP are very similar, being $n = 1.16 \pm 0.05$, $k = (1.52 \pm 0.09) \times 10^{-3}$ min^{-1} for eq 1 and $n = 1.29 \pm 0.03$, $k = (1.23 \pm 0.03) \times 10^{-3}$ min^{-1} for eq 2.

These results were not obvious, since $\alpha_{\tau'\text{-ZrP}}$ and $\alpha_{\alpha\text{-ZrP}}$ were calculated by using independent data, so that it is possible to infer that the disapperance of the anhydrous α-ZrP phase is reasonably due to its direct transformation into the τ'-ZrP phase.

Another interesting aspect is the stability of the τ'-ZrP phase. Figure 12 shows the XRPD pattern of *propanol_6_120* (a) and

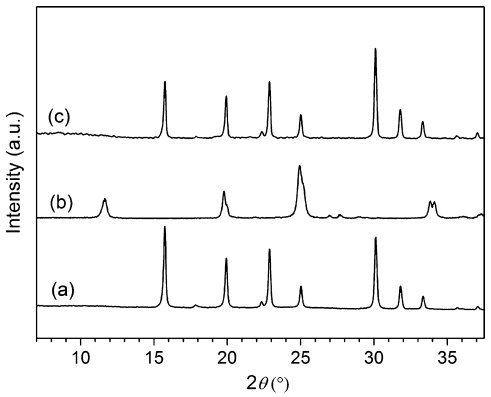

Figure 12. X-ray diffraction patterns of: fresh *propanol_6_120* (a); *propanol_6_120* equilibrated at 53% RH at room temperature for one week (b); *propanol_6_120* washed with anhydrous ethanol and equilibrated at 53% RH at room temperature for one week (c).

that of the same sample after equilibration at 53% relative humidity (RH) at room temperature for one week, pattern (b), which, surprisingly, corresponds to that of α-ZrP·H_2O, indicating that the τ'-ZrP → α-ZrP·H_2O phase transistion occurs in these conditions. TEM images prove that, during this transformation, the sample progressively changes from a compact to a layered morphology (Figure 13). The same transition was not observed when *propanol_6_120* was previously washed with anhydrous ethanol, pattern (c) of Figure 12.

It is interesting to observe that when *propanol_6_60* is also washed with anhydrous ethanol, then the α-ZrP·H_2O → τ'-ZrP phase transition does not occur at 120 °C. To get insight into the factors responsible for the α-ZrP·H_2O ⇆ τ'-ZrP transition, one should remember that, before washing, the P/Zr molar ratio for the above samples was ∼2.3, due to the presence of a certain amount of free phosphoric acid, while the P/Zr molar ratio for both *propanol_6_60* and *propanol_6_120* washed with anhydrous ethanol (hereafter indicated as *stabilized* τ'-ZrP and *stabilized* α-ZrP·H_2O, respectively) was ∼2. On the basis of these results it can be inferred that the α-ZrP·H_2O ⇆ τ'-ZrP transition occurs in the presence of free phosphoric acid, and when it is removed by washing with anhydrous ethanol, the above transition is inhibited. All these observations are summarized according to Scheme 1.

The reversibility of the α-ZrP·H_2O ⇆ τ'-ZrP transition in the presence of free phosphoric acid may reasonably be justified by considering that

DOI: 10.1021/acs.inorgchem.5b01573
Inorg. Chem. 2015, 54, 9146–9153

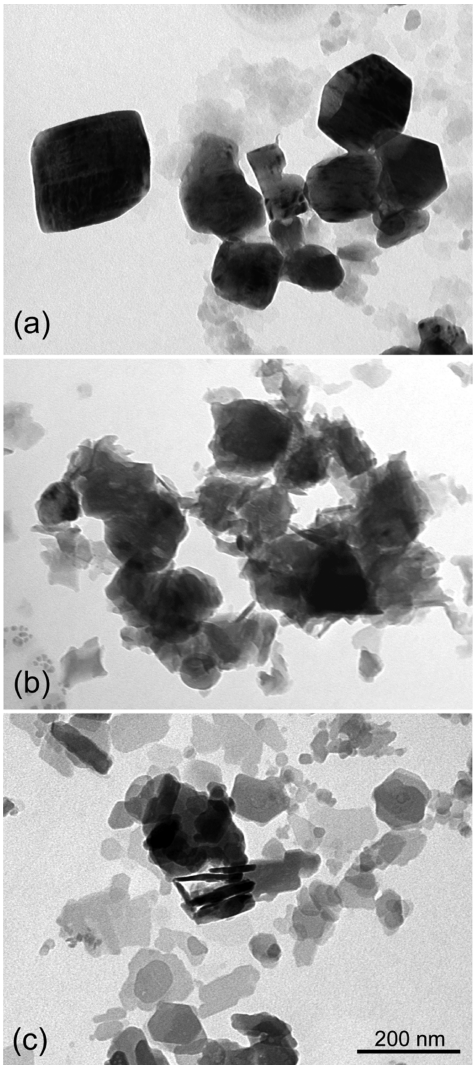

Figure 13. TEM images of fresh *propanol_6_120* (a), the same sample equilibrated at 53% RH at room temperature for 1 d (b) and for one week (c).

- Phosphoric acid can act as catalyst for the transformation of α-ZrP·H_2O into τ'-ZrP at 120 °C, probably due to its acidity that may increase the mobility of HPO_4 groups, through a protonation−deprotonation pathway, inside the structure;
- Phosphoric acid can also act as catalyst for the conversion of τ'-ZrP into α-ZrP·H_2O at room temperature and 53% RH, also beacuse of its hygroscopicity, which is expected to promote the water absorption and, consequently, the formation of the phase thermodynamically more stable at room temperature, that, is α-ZrP·H_2O. However, it should be remarked that the presence of free phosphoric acid is not able to promote a similar behavior when it is physically mixed with both microcrystalline α-ZrP or *stabilized* nanocrystalline α-ZrP in a corresponding ratio. As a matter of fact, by heating at 120 °C a microcrystalline α-ZrP/H_3PO_4 or a *stabilized* nanocrystalline α-ZrP/H_3PO_4 physical mixture for 15 h, the formation of the τ'-ZrP phase was not observed in that range of time.

Therefore, it can be concluded that nanosized α-ZrP is, at least kinetically, more reactive than microcrystalline α-ZrP, probably due to its higher surface area and to the presence of structural defects.[3a]

4. CONCLUSIONS

The present study revealed that α-ZrP nanocrystals, obtained from gels of nanosized α-ZrP in propanol, have a different thermal behavior as compared to microcrystalline α-ZrP. Specifically, nanocrystalline α-ZrP undergoes an unusual phase transition at 120 °C, leading to a new phase with a 3D structure. This new compound, consisting of nanoparticles with a cubelike morphology and size of hundreds of nanometers, has been called τ'-ZrP, due to its structural similarities with the already known τ-ZrP phase.

Kinetic studies, according to the JMAK model, proved that the α-ZrP·H_2O → τ'-ZrP occurred by direct transformation of the layered structure into the 3D structure.

Moreover, it has been found that the transformation of α-ZrP·H_2O into τ'-ZrP, as well as the reverse reaction, takes place in the presence of free phosphoric acid (originally present in nanosized α-ZrP), which acts as a catalyst. As a matter of fact, the above transition does not occur when phosphoric acid is removed from nanosized α-ZrP·H_2O by washing with anhydrous ethanol. It is also noteworthy that the above phase transition is not observed by heating at 120 °C microcrystalline α-ZrP·H_2O in the presence of free phosphoric acid, thus establishing the unusual reactivity and versatility of α-ZrP nanocrystals.

■ ASSOCIATED CONTENT

Supporting Information

The Supporting Information is available free of charge on the ACS Publications website at DOI: 10.1021/acs.inorgchem.5b01573.

Crystal data for τ'-ZrP. (CIF)

Scheme 1. Reaction Pathways for Nanosized α-ZrP·H_2O and τ'-ZrP

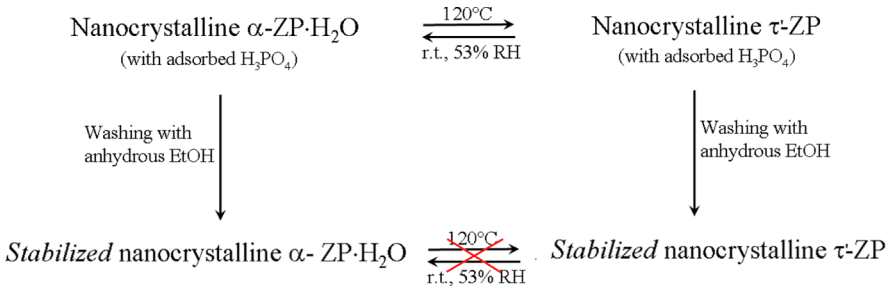

DOI: 10.1021/acs.inorgchem.5b01573
Inorg. Chem. 2015, 54, 9146−9153

AUTHOR INFORMATION

Corresponding Author

*E-mail: monica.pica@unipg.it. Phone: +39 075 585 5564. Fax: +39 075 585 5566.

Notes

The authors declare no competing financial interest.

REFERENCES

(1) Clearfield, A.; Costantino, U. In *Comprehensive Supramolecular Chemistry;* Alberti, G., Bein, T., Eds.; Pergamon, Elsevier Science Ltd. Press: New York, 1996; Vol. *7*, Chapter 4.

(2) (a) Kumar, C. V.; Chaudhari, A. *J. Am. Chem. Soc.* **2000**, *122*, 830−837. (b) Alberti, G.; Costantino, U. *J. Mol. Catal.* **1984**, *27*, 235−250. (c) Alberti, G.; Casciola, M.; Costantino, U.; Levi, G.; Ricciardi, G. *J. Inorg. Nucl. Chem.* **1978**, *40*, 533−537. (d) Diaz, A.; Saxena, V.; Gonzalez, J.; David, A.; Casanas, B.; Carpenter, C.; Batteas, J. D.; Colón, J. L.; Clearfield, A.; Hussain, M. D. *Chem. Commun.* **2012**, *48*, 1754−1756. (e) Bellezza, F.; Cipiciani, A.; Costantino, U.; Nicolis, S. *Langmuir* **2004**, *20*, 5019−5025. (f) Emig, G.; Hofmann, H. *J. Catal.* **1983**, *84*, 15−26. (g) Sue, H. J.; Gam, K. T.; Bestaoui, N.; Spurr, N.; Clearfield, A. *Chem. Mater.* **2004**, *16*, 242−249. (h) Alberti, G.; Casciola, M.; Capitani, D.; Donnadio, A.; Narducci, R.; Pica, M.; Sganappa, M. *Electrochim. Acta* **2007**, *52*, 8125−8132. (i) Casciola, M.; Capitani, D.; Comite, A.; Donnadio, A.; Frittella, V.; Pica, M.; Sganappa, M.; Varzi, A. *Fuel Cells* **2008**, *8*, 217−224. (j) Casciola, M.; Alberti, G.; Donnadio, A.; Pica, M.; Marmottini, F.; Bottino, A.; Piaggio, P. *J. Mater. Chem.* **2005**, *15*, 4262−4267. (k) Arbizzani, C.; Donnadio, A.; Pica, M.; Sganappa, M.; Varzi, A.; Casciola, M.; Mastragostino, M. *J. Power Sources* **2010**, *195*, 7751−7756. (l) Pica, M.; Donnadio, A.; Casciola, M.; Cojocaru, P.; Merlo, L. *J. Mater. Chem.* **2012**, *22*, 24902−24908. (m) Pica, M.; Donnadio, A.; Casciola, M. *Starch/Stärke* **2012**, *64*, 237−245. (n) Sun, L.; Boo, W. J.; Sun, D.; Clearfield, A.; Sue, H. J. *Chem. Mater.* **2007**, *19*, 1749−1754. (o) Petrucci, C.; Cappelletti, M.; Piermatti, O.; Nocchetti, M.; Pica, M.; Pizzo, F.; Vaccaro, L. *J. Mol. Catal. A: Chem.* **2015**, *401*, 27−34. (p) Pica, M.; Nocchetti, M.; Ridolfi, B.; Donnadio, A.; Costantino, F.; Gentili, P. L.; Casciola, M. *J. Mater. Chem. A* **2015**, *3*, 5525−5534.

(3) (a) Pica, M.; Donnadio, A.; Capitani, D.; Vivani, R.; Troni, E.; Casciola, M. *Inorg. Chem.* **2011**, *50*, 11623−11630. (b) Sun, L.; Boo, W. J.; Sue, H. J.; Clearfield, A. *New J. Chem.* **2007**, *31*, 39−43. (c) Capitani, D.; Casciola, M.; Donnadio, A.; Vivani, R. *Inorg. Chem.* **2010**, *49*, 9409−9415. (d) Jiménez-Jiménez, J.; Maireles-Torres, P.; Olivera-Pastor, P.; Rodríguez-Castellón, E.; Jiménez-López, A.; Jones, D. J.; Rozière, J. *Adv. Mater.* **1998**, *10*, 812−815. (e) Wang, D.; Yu, R.; Kumada, N.; Kinomura, N. *Chem. Mater.* **2000**, *12*, 956−960. (f) Liu, L.; Yang, J.; Li, J.; Dong, J.; Šišak, D.; Luzzatto, M.; McCusker, L. *Angew. Chem., Int. Ed.* **2011**, *50*, 8139−8142.

(4) (a) Pica, M.; Donnadio, A.; Troni, E.; Capitani, D.; Casciola, M. *Inorg. Chem.* **2013**, *52*, 7680−7687. (b) Pica, M.; Donnadio, A.; D'Amato, R.; Capitani, D.; Taddei, M.; Casciola, M. *Inorg. Chem.* **2014**, *53*, 2222−2229.

(5) (a) Pica, M.; Donnadio, A.; Casciola, M.; Cojocaru, P.; Merlo, L. *J. Mater. Chem.* **2012**, *22*, 24902−24908. (b) Casciola, M.; Cojocaru, P.; Donnadio, A.; Giancola, S.; Merlo, L.; Nedellec, Y.; Subianto, S.; Pica, M. *J. Power Sources* **2014**, *262*, 407−413.

(6) Werner, P. E.; Eriksson, L.; Westdahl, M. *J. Appl. Crystallogr.* **1985**, *18*, 367−370.

(7) Boultif, A.; Louer, D. *J. Appl. Crystallogr.* **1991**, *24*, 987−993.

(8) Favre-Nicolin, V.; Cerny, R. *J. Appl. Crystallogr.* **2002**, *35*, 734−743.

(9) Falcioni, M.; Deem, M. W. *J. Chem. Phys.* **1999**, *110*, 1754−1766.

(10) Larson, A. C.; Von Dreele, R. B. *Generalized Crystal Structure Analysis System;* Los Alamos National Laboratory: Los Alamos, NM, 2001.

(11) Clearfield, A.; Landis, A. L.; Medina, A. S.; Troup, J. M. *J. Inorg. Nucl. Chem.* **1973**, *35*, 1099−1108.

(12) Segawa, K.; Kurusu, Y.; Nakajima, Y.; Kinoshita, M. *J. Catal.* **1985**, *94*, 491−500.

(13) Krogh Andersen, A. M.; Norby, P.; Hanson, J. C.; Vogt, T. *Inorg. Chem.* **1998**, *37*, 876−881.

(14) De Wolff, P. M. *J. Appl. Crystallogr.* **1968**, *1*, 108−113.

(15) Laugier, J.; Bochu, B. *LMGP-Suite;* ENSP/Laboratoire des Matériaux et du Génie Physique: Saint Martin d'Hères, France.

(16) Clearfield, A. *Annu. Rev. Mater. Sci.* **1984**, *14*, 205−229.

(17) (a) Kolmogrov, A. N. *Sci. Math. Nat.* **1937**, *3*, 355−359. (b) Avrami, M. *J. Chem. Phys.* **1940**, *8*, 212−224. (c) Johnson, W. A.; Mehl, R. F. *Trans. Am. Inst. Min., Metall. Pet. Eng.* **1939**, *135*, 416−441.

DOI: 10.1021/acs.inorgchem.5b01573
Inorg. Chem. 2015, 54, 9146−9153